MgCeAl$_{11}$O$_{19}$:Tb^{3+} and Mg$_8$Ge$_2$O$_{11}$F$_2$:Mn^{4+} in enhancing the color quality of remote phosphor LED

My Hanh Nguyen Thi[1], Phung Ton That[2]
[1]Faculty of Mechanical Engineering, Industrial University of Ho Chi Minh City, Vietnam
[2]Faculty of Electronics Technology, Industrial University of Ho Chi Minh City, Vietnam

Article Info	ABSTRACT
	As the name infers, the triple-layer remote phosphor (TRP) has 3 phosphor layers includes the red Mg$_8$Ge$_2$O$_{11}$F$_2$:Mn^{4+} phosphor layer on the top, the green MgCeAl$_{11}$O$_{19}$:Tb^{3+} phosphor layer in the middle, and the yellow YAG:Ce^{3+} layer at the bottom and is mentioned as a solution to increase the chromaticity and luminescence adequacy of the white LEDs (WLEDs) in this article. As to control the red light for higher value achieve in the color rendering index (CRI), using red Mg$_8$Ge$_2$O$_{11}$F$_2$:Mn^{4+} phosphor in the TRP structure is recommended. All the outcomes indicate that when red phosphor Mg$_8$Ge$_2$O$_{11}$F$_2$:Mn^{4+} concentration grows the CRI gets higher values, and drastically declines when the concentration of green phosphor MgCeAl$_{11}$O$_{19}$:Tb^{3+} increases. As the same time, applying the green MgCeAl$_{11}$O$_{19}$:Tb^{3+} phosphor layer to manage the green light as it can make the luminous efficacy (LE) of WLEDs increase. In particular, the index of LE can also be improved over 40% by limiting the scatter of light and putting in green light. Moreover, to preserve the average correlated color temperature (ACCT) stable at 8500K, the yellow YAG:Ce^{3+} concentration must be cut down as the concentration of red and green phosphor rise.

Corresponding Author:

Phung Ton That
Faculty of Electronics Technology
Industrial University of Ho Chi Minh City
No. 12 Nguyen Van Bao Street, Ho Chi Minh City, Vietnam
Email: tonthatphung@iuh.edu.vn

1. INTRODUCTION

Phosphor-converted white light-emitting diodes (WLEDs), a promising light source with numerous remarkable attributes including being the compact, power saving, cost effective, and color consistency, have received increasing popularity in illumination market [1-3]. WLEDs are manufactured by applying the complementary colors principle, merging blue lights from a blue LED chip and yellow lights from phosphor [4]. The most well-known technique to produce white light is to employ the freely dispersed coating. In this process, the transparent encapsulated resin and the phosphor powder are blended together then scattered on the phosphor layers. The method provides control over the thickness of phosphor and is low cost, however, cannot achieve high quality WLEDs due to low luminous efficiency. Therefore, WLEDs can possibly participate in solid-state lighting should their lumen efficacy is improved [5]. The conformal coating method is proposed to supports color uniformity and leads to the uniformity of angular-dependent correlated color temperature (CCT) [6], but the light loss from backscattering effect prevents it from becoming the optimal solution. In attempts to achieve the higher luminescence for WLEDs to meet the lighting standard of solid-

state lighting, prior researches have proposed many methods. For example, a remote phosphor packaging structures to isolate the chip and the phosphor layer [7-12], a reflection structure that has an interior phosphor coating on polymer hemispherical shell lens to boost extraction efficiency, an air-gap embedded structure to boost luminous efficacy by reflecting downward light. In addition, limiting the loss of light from backscattering and enhance the dispersal of blue and yellow lights are crucial objectives in making greater quality WLEDs. In terms of luminous efficiency, the concentration of the phosphor is as important as the structure of the package [13-17]. The re-absorption loss in the phosphor and the phosphor concentration are related to each other, which means if one aspect rises it will cause an increase in others. Hence, the luminous efficiency of the device decline, particularly in WLEDs with lower CCTs [18-20]. Based on the information mentioned above, this paper presents the triple-layer remote phosphor WLEDs that has color temperature of 8500 K that will be tested with different concentration of phosphor as a solution. The components of the TRP structure are three separate phosphor layers, the green $MgCeAl_{11}O_{19}:Tb^{3+}$ phosphor layer in between the yellow $YAG:Ce^{3+}$ phosphor layer at the bottom and red $Mg_8Ge_2O_{11}F_2:Mn^{4+}$ phosphor layer on top. The function of the green phosphor layer is to support the green light components and enhance photon emission. The red phosphor layer, on the other hand, improves red light component for better color quality. The results suggest that despite the insignificant decrease in WLEDs luminous flux, the TRP structure allows yellow, green, and red color proportions to be balanced and reach the highest potential. Such information is great news especially in the WLEDS industry that demands constant changes.

2.   PREPARATION AND SIMULATION

Red phosphor $Mg_8Ge_2O_{11}F_2:Mn^{4+}$ and green phosphor $MgCeAl_{11}O_{19}:Tb^{3+}$ are used in this research because they are low-cost, easy to produce and apply. These phosphors are applied to two purposes, the first one is to improve the WLEDs luminous flux with the green light component from $MgCeAl_{11}O_{19}:Tb^{3+}$ layer. The second one is raising color rendering index (CRI) and color quality ratio (CQS) values with red $Mg_8Ge_2O_{11}F_2:Mn^{4+}$ phosphor layer providing more red-light components in WLEDs.

As shown in Figure 1 (a), the WLEDs in this study present the best optical-thermal stability. We have them built very carefully so that they identical to each other. This physical model of WLEDs has a reflector that is 2.07 mm in height, 9.85 mm in length at its top surface and an 8 mm long bottom. The remote phosphor layer has a fixed thickness of 0.08 mm and covers 9 LED chips. Each LED chip is 1.14 mm square base, has the height of 0.15 mm and bound to the cavity on the reflector. The output of each blue chip is 1.16W at 453 nm wavelength. The normalized cross correlations between them are approximately 99.6%, which means the real packaging and the one used for the simulation are similar. In addition, lower the influences from different elements such as LED wavelength, waveform, light intensity, and operating temperature on the CRI and CCT. The Monte Carlo ray-tracing method based commercial software, LightTools 8.1.0, is employed to replicate the WLEDs with the remote phosphor structure and average CCT values of 6000 K, 7000 K, and 8500 K. Figure 1 (b) displays the 2-D simulated physical model of WLEDs use to perform optical simulations of remote package WLEDs. The concentration of phosphor particles varies constantly from 2% to 20%. Yet, by controlling the $YAG:Ce^{3+}$ wt. concentration the average CCT values are remained the same.

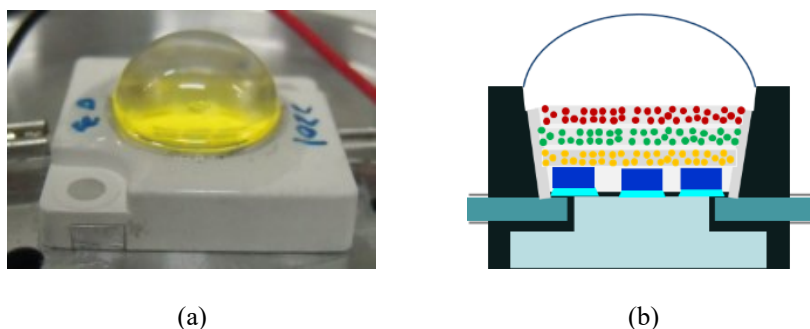(a)   (b)

Figure 1. (a) WLEDs, and (b) Illustration of triple-layer remote phosphor configuration

3.   RESULTS AND DISCUSSION

As shown in Figure 2, the red phosphor and green phosphor concentrations in the range of 2% to 20% contribute to the modification of CRI. The CRI rises up if red phosphor concentration goes up and

achieves the highest value when red phosphor concentration is at 20%. On the contrary, adding in green phosphor is not beneficial for the CRI. The results show that disregard to the addition of red phosphor or alteration in average correlated color temperature (ACCT), when the green phosphor increases from 2% to 20%, the CRI value will decrease accordingly. Therefore, adding the red-light component in WLEDs, which is generated from red $Mg_8Ge_2O_{11}F_2:Mn^{4+}$ phosphor layer, is crucial to boosting CRI value while increasing the green $MgCeAl_{11}O_{19}:Tb^{3+}$ phosphor concentration is unfavorable for the CRI. The problems are the growth of green phosphor reduces the conversion energy in the red phosphor layer and emitted light only gets to the red phosphor once passing through the green phosphor due to packaging order. Therefore, to achieve better CRI value, the green $MgCeAl_{11}O_{19}:Tb^{3+}$ phosphor concentration should be reduced as low as possible. However, CRI is not the only indicator for color quality. The viewer's preference and the color coordinates are the two fundamental criteria besides the true color of the object that are not covered by the CRI. Color quality scale (CQS), on the other hand, contains three components: CRI, visual preference, and color coordinates for white light [20]. Therefore, when in comparison with CRI, CQS stands out as the more noteworthy and more challenging goal to accomplish. Then it leads to the question of how to improve the CQS value in WLEDs? Is it similar to the CRI and red-light component is the only thing that is needed to improve the value? The explanation is in Figure 3, in which the CQS is analyzed into details.

Generally, CQS also benefits from the growth of the red $Mg_8Ge_2O_{11}F_2:Mn^{4+}$ phosphor concentration. However, the deflection of CQS is less significant than that of CRI when green phosphor $MgCeAl_{11}O_{19}:Tb^{3+}$ concentration varies, in particular, the CQS only decrease when the green phosphor concentration exceeds 14%. As can be seen from Figure 3, both green phosphor and red phosphor can enhance CQS. The key point in improving CQS is the balance among three color components: green, yellow, and red. As to maintain the ACCT level, when the concentrations of green and red phosphors increase, the yellow phosphor concentration will drop.
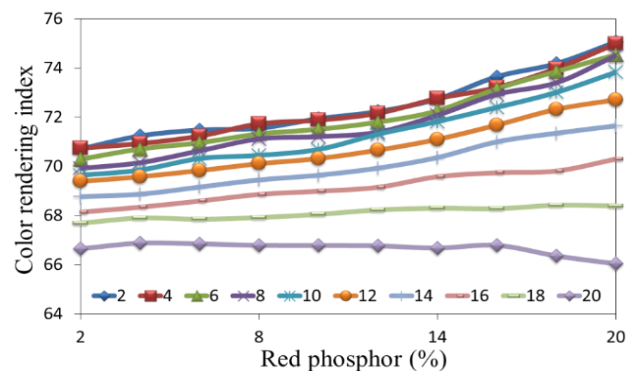

Figure 2. CRI in TRP with red $Mg_8Ge_2O_{11}F_2:Mn^{4+}$ phosphor and green $MgCeAl_{11}O_{19}:Tb^{3+}$ phosphor
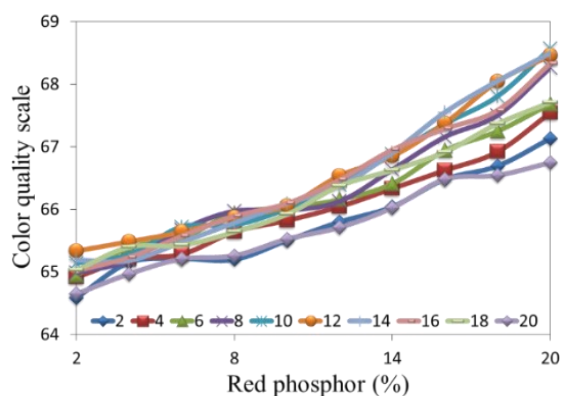
Figure 3. CQS of TRP as a function of red $Mg_8Ge_2O_{11}F_2:Mn^{4+}$ phosphor and green $MgCeAl_{11}O_{19}:Tb^{3+}$ phosphor

As mentioned, the yellow-green-red color balance is the key to improve CQS. Hence, controlling CQS means controlling the balance between the three colors. This can be achieved by applying the results in

Figure 3, which show CQS values grow as green MgCeAl$_{11}$O$_{19}$:Tb^{3+} phosphor increases in the range of 2% to 10% and the highest values of CQS is achieved when green phosphor MgCeAl$_{11}$O$_{19}$:Tb^{3+} in between 10% to 14%. These events are because when the concentration of the green phosphor is low (2% to 10%), the composition of yellow light still dominates, therefore, the loss of light-transmitting energy by scattering leads to high CQS and when the green concentration is from 10% to 14%, green light is a necessity to reach the peak value of CQS. However, as the MgCeAl$_{11}$O$_{19}$:Tb^{3+} keeps increasing, the excessive green light deflects the balance among the three colors red, green, and yellow, causing a reduction in CQS.

It is much more difficult to control the color quality of the remote phosphor structure than the conformal phosphor or in-cup phosphor structures. Adjusting the color quality in WLEDs with ACCT of 8500 K is also more challenging. However, in the TRP structure, it can be seen that the higher the ACCT, the greater the CQS. Moreover, TRP structure also increases light scattering inside WLEDs and limits the volume of scattered light, which supports the combination of light components, resulting in the production of white light with advance quality. However, will the light energy be affected by this enhancement of scattering?

This part introduces and illustrates the numerical model of the transmitted blue light and converted yellow light in the double-layer phosphor structure, from which changes can be made to create immense enhancement to LED efficiency. The blue light transmission and the conversion of yellow light in single layer remote phosphor package with the phosphor layer thickness of 2h expressed as (1) and (2) [21-26].

$$PB_1 = PB_0 \times e^{-2\alpha_{B1}h} \tag{1}$$

$$PY_1 = \frac{1}{2}\frac{\beta_1 \times PB_0}{\alpha_{B1} - \alpha_{Y1}}(e^{-2\alpha_{Y1}h} - e^{-2\alpha_{B1}h}) \tag{2}$$

In double layer remote phosphor package with the phosphor layer thickness of h the blue light transmission and the conversion of yellow light are defined as:

$$PB_2 = PB_0 \times e^{-2\alpha_{B2}h} \tag{3}$$

$$PY_2 = \frac{1}{2}\frac{\beta_2 \times PB_0}{\alpha_{B2} - \alpha_{Y2}}(e^{-2\alpha_{Y2}h} - e^{-2\alpha_{B2}h}) \tag{4}$$

The thickness of every phosphor layer is represented by h. The subscript "1" and "2" depict single layer and double-layer remote phosphor package. β presents the conversion coefficient from blue light to yellow light. γ represent the reflection coefficient of the yellow light. The light intensity from the blue LED are the intensities of blue light (PB) and yellow light (PY), demonstrated by PB_0. α_B; α_Y which are parameters depicting the portion of the blue and yellow lights energy loss in their diffusion process in the phosphor layer. The pc-LEDs lighting efficiency develops significantly in the double-layer phosphor structure compared to a single layer structure:

$$\frac{(PB_2 + PY_2) - (PB_1 + PY_1)}{PB_1 + PY_1} > 0 \tag{5}$$

The scattering of phosphor particles was tested with the Mie-theory. In addition, by applying the Mie theory, the scattering cross section C_{sca} for spherical particles can be calculated with the following expression. The transmitted light power can be measured by the Lambert-Beer law [22] as shown in (6). In which I_0 is the incident light power, L is the thickness of phosphor layer (mm) and μ_{ext} is the extinction coefficient, which can be expressed as: $\mu_{ext} = N_r.C_{ext}$, where N_r is as the number density distribution of particles (mm^{-3}). C_{ext} (mm^2) is the extinction cross-section of phosphor particles.

$$I = I0\ exp(-\mu extL) \tag{6}$$

The (5) indicates that the luminous emission of WLEDs benefits from the utilization of many phosphor layers. The red phosphor and green phosphor concentrations are increased with the development of luminous emission. Therefore, to stabilize the ACCTs, the concentration of yellow phosphor must drop as the concentrations of red phosphor and green phosphor rise. The reduction of yellow phosphor concentration serves the purpose of limiting the light energy comes from scattering. In addition, as stated in the Lambert-Beer law in (6), the concentration of yellow phosphor declines as the transmitted light power rises. Accordingly, the higher concentration of the phosphoric MgCeAl$_{11}$O$_{19}$:Tb^{3+} layer or Mg$_8$Ge$_2$O$_{11}$F$_2$:Mn^{4+}, the

larger luminous flux output, unfortunately, that is unfavorable for CQS. The excessive amount of red or green light will induce inequality between the three colors, thus, leads to deterioration in CQS.

As it is shown in Figure 4, luminous emission (LE) is able to move up 40% due to the addition of green light and scattered light scattering from the $MgCeAl_{11}O_{19}:Tb^{3+}$ phosphor layer. The concentration of $Mg_8Ge_2O_{11}F_2:Mn^{4+}$ in 8500 K ACCT WLED also influence a bit on the enhancement of LE. However, with the concentration of $Mg_8Ge_2O_{11}F_2:Mn^{4+}$ within 2-14%, the LE values remain unvaried. Then when green phosphor concentration reaches 20% LE begins to fall off slightly. The result of this research is valuable information for manufacturers to find the most optimal concentration for these phosphors. For instance, the manufacturers can choose the $MgCeAl_{11}O_{19}:Tb^{3+}$ concentration 10% to 14% with $Mg_8Ge_2O_{11}F_2:Mn^{4+}$ concentration at 20% for the high CQS and LE.
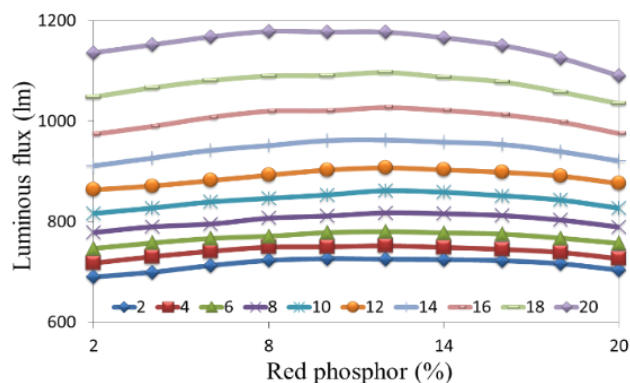

Figure 4. Luminous flux of TRP as a function of red $Mg_8Ge_2O_{11}F_2:Mn^{4+}$ phosphor and green $MgCeAl_{11}O_{19}:Tb^{3+}$ phosphor

4. CONCLUSION

In summary, the TRP structure, which contains the green phosphor layer $MgCeAl_{11}O_{19}:Tb^{3+}$ and the red phosphor layer $Mg_8Ge_2O_{11}F_2:Mn^{4+}$, was mentioned as an optimal solution to improve the CRI, CQS, and LE of WLEDs. The TRP structure has proved to not only enhance the color quality but also increase LE, a result that has never seen before. In order for that to happen, a balance between the three colors: red, green and yellow in the phosphor layers needs to be created by influencing the concentration in $MgCeAl_{11}O_{19}:Tb^{3+}$ and $Mg_8Ge_2O_{11}F_2:Mn^{4+}$. Managing the green light component from the green $MgCeAl_{11}O_{19}:Tb^{3+}$ phosphor layer in WLEDs is crucial for the improvement of luminous flux. Besides, when dealing with the concentration of the red $Mg_8Ge_2O_{11}F_2:Mn^{4+}$ layer, the red light component in WLEDs is the key to control the CRI. Moreover, the usage of several layers of phosphor instead of a single layer is more beneficial to the enhancement of luminous flux. The results of the study provide a configuration to the best color quality and luminescence WLEDs with outstanding attributes that can satisfy the people's demands.

REFERENCES

[1] M. M. Magno-Canto *et al.*, "Model for deriving benthic irradiance in the Great Barrier Reef from MODIS satellite imagery," *Opt. Express,* vol. 27, no. 20, pp. A1350-A1371, 2019.

[2] I. G. Palchikova *et al.*, "Quantization noise as a determinant for color thresholds in machine vision," *J. Opt. Soc. Am. A,* vol. 35, no. 4, pp. B214-B222, 2018.

[3] T. Kozacki *et al.*, "Fourier rainbow holography," *Opt. Express,* vol. 26, no. 19, pp. 25086-25097, 2018.

[4] S. W. Jeon *et al.*, "Optical design of dental light using a remote phosphor light-emitting diode package for improving illumination uniformity," *Appl. Opt*, vol. 57, no. 21, pp. 5998-6003, 2018.

[5] Y. T. Wang *et al.*, "Color conversion efficiency enhancement of colloidal quantum dot through its linkage with synthesized metal nanoparticle on a blue light-emitting diode," *Opt. Lett*, vol. 44, no. 23, pp. 5691-5694, 2019.

[6] Y. Tang *et al.*, "Enhancement of luminous efficacy for LED lamps by introducing polyacrylonitrile electrospinning nanofiber film," *Opt. Express,* vol. 26, no. 21, pp. 27716-27725, 2018.

[7] P. Zhu *et al.*, "Design of circadian white light-emitting diodes with tunable color temperature and nearly perfect color rendition," *OSA Continuum,* vol. 2, no. 8, pp. 2413-2427, 2019.

[8] A. J. Henning *et al.*, "Improvements to dispersed reference interferometry: beyond the linear approximation," *Appl. Opt*, vol. 58, no. 1, pp. 131-136, 2019.

[9] C. Zhang *et al.*, "Mn^{4+}-doped fluoride phosphors rapidly synthesized by ball milling," *Opt. Mater. Express,* vol. 8, no. 1, pp. 73-81, 2018.

[10] X. Bao *et al.*, "User-centric quality of experience optimized resource allocation algorithm in VLC network with multi-color LED," *Opt. Express,* vol. 26, no. 21, pp. 27826-27841, 2018.

[11] J. Cheng *et al.*, "Luminescence and energy transfer properties of color-tunable Sr_4La , $PO_{4.3}O$: Ce^{3+}, Tb^{3+}, Mn^{2+} phosphors for WLEDs," *Opt. Mater. Express,* vol. 8, no. 7, pp. 1850-1862, 2018.

[12] X.Yuan *et al.*, "Ultra-high capacity for three-dimensional optical data storage inside transparent fluorescent tape," *Opt. Lett*, vol. 45, no. 6, pp. 1535-1538, 2020.

[13] W. Wang *et al.*, "Red photoluminescent Eu3+-doped Y2O3 nanospheres for LED-phosphor applications: Synthesis and characterization," *Opt. Express,* vol. 26, no. 26, pp. 34820-34829, 2018.

[14] P. Kumar *et al.*, "Enhanced exclusive-OR and quick response code-based image encryption through incoherent illumination," *Appl. Opt*, vol. 58, no. 6, pp. 1408-1412, 2019.

[15] A. Motazedifard *et al.*, "Measurement of thickness of thin film by fitting to the intensity profile of Fresnel diffraction from a nanophase step," *J. Opt. Soc. Am. A,* vol. 35, no. 12, pp. 2010-2019, 2018.

[16] R. E. O'Shea *et al.*, "Evaluation of glint correction approaches for fine-scale ocean color measurements by lightweight hyperspectral imaging spectrometers," *Appl. Opt*, vol. 59, no. 7, pp. B18-B34, 2020.

[17] Y. Xie *et al.*, "Encapsulated room-temperature synthesized CsPbX3 perovskite quantum dots with high stability and wide color gamut for display," *Opt. Mater. Express,* vol. 8, no. 11, pp. 3494-3505, 2018.

[18] L. Duan *et al.*, "Wide color gamut display with white and emerald backlighting," *Appl. Opt*, vol. 57, no. 6, pp. 1338-1344, 2018.

[19] Y. L. Piao *et al.*, "Chromatic-dispersion-corrected full-color holographic display using directional-view image scaling method," *Appl. Opt*, vol. 58, no. 5, pp. A120-A127, 2019.

[20] J. J. Gómez-Valverde *et al.*, "Automatic glaucoma classification using color fundus images based on convolutional neural networks and transfer learning," *Biomed. Opt. Express,* vol. 10, no. 2, pp. 892-913, 2019.

[21] C. Zhang *et al.*, "Exciton photoluminescence of $CsPbBr_3@SiO_2$ quantum dots and its application as a phosphor material in light-emitting devices," *Opt. Mater. Express,* vol. 10, no. 4, pp. 1007-1017, 2020.

[22] G. Prabhakar *et al.*, "Octave-wide supercontinuum generation of light-carrying orbital angular momentum," *Opt. Express,* vol. 27, no. 8, pp. 11547-11556, 2019.

[23] Y. Peng *et al.*, "Flexible fabrication of a patterned red phosphor layer on a YAG:Ce3+ phosphor-in-glass for high-power WLEDs," *Opt. Mater. Express,* vol. 8, no. 3, pp. 605-614, 2018.

[24] Z. Zhuang *et al.*, "Optimal ITO transparent conductive layers for InGaN-based amber/red light-emitting diodes," *Opt. Express,* vol. 28, no. 8, pp. 12311-12321, 2020.

[25] N. Q. Li *et al.*, "High-efficiency solution-processed WOLEDs with very high color rendering index based on a macrospirocyclic oligomer matrix host," *Opt. Mater. Express,* vol. 8, no. 10, pp. 3208-3219, 2018.

[26] J. Jia *et al.*, "Three-wavelength passive demodulation technique for the interrogation of EFPI sensors with arbitrary cavity length," *Opt. Express,* vol. 27, no. 6, pp. 8890-8899, 2019.